Texturing the cathode of white organic light-emitting diodes with a lattice of nanoscale scatterers for enhanced light out-coupling

Ardavan Oskooi[a)]
Department of Electrical Engineering and Computer Science, University of Michigan, Ann Arbor, Michigan 48109, USA

(Received 13 November 2014; accepted 16 January 2015; published online 28 January 2015)

The external quantum efficiency of white organic light-emitting diodes is often limited by light out-coupling losses due to surface plasmons. We demonstrate how texturing of the metal-cathode surface using a two-dimensionally periodic lattice of nanoscale scatterers with limited disorder can be used to reduce plasmonic losses while simultaneously enhancing both the light out-coupling and the spontaneous-emission rate of the excitons. We use electrodynamic simulations and statistical modeling to explore the relationship between the topology of the surface texture and its corresponding scattering efficiency. From this, we outline attributes of textures that can most enhance device performance. © *2015 AIP Publishing LLC*. [http://dx.doi.org/10.1063/1.4907253]

The development of organic light-emitting diodes (OLEDs), particularly those based on small-molecule phosphorescent materials,[1] has led to a number of commercial applications arising from their nearly 100% internal quantum efficiency (IQE). Yet the external quantum efficiency (EQE), which takes into account the light-extraction efficiency, still has significant room for improvement despite intensive work based on a number of different designs including microlens arrays, low-index microstructured grids, high-index substrates, oriented-dipole emitters, photonic crystals, and plasmonic out-coupling schemes.[2,3] In this work, we describe a design for a nanostructured, white-emitting OLED (WOLED), operating under the conditions of broad spectral bandwidth and isotropic emitters, which enhances both the light-extraction efficiency and the spontaneous-emission rate of the excitons.[4–8] Our approach, which does not require any additional materials, involves applying a texture to the metal-cathode surface where its topology consists of a two-dimensionally periodic lattice of nanoscale scatterers augmented with limited disorder. This design fulfills two objectives: (1) to enhance *coupling* to the surface-plasmon polaritons (SPPs) to boost the rate of exciton decay and (2) to radiatively *scatter* out as many of these otherwise non-radiative modes over the shortest possible distance. We employ a three-dimensional electromagnetic solver[9,10] to simulate the optical properties of a WOLED by statistically modeling the temporal dynamics of exciton recombination and with this show that while there is some degree of flexibility in the choice of the morphology of the scatterers and the topology of the lattice, their exact dimensions must be carefully tuned to optimize device performance.

While several previous works have focused on reducing losses from surface plasmons via texturing,[11–16] there appears to be a lack of designs for reducing such losses while simultaneously enhancing the light-extraction efficiency and the spontaneous-emission rate of excitons compared to an unpatterned device. Our work is used to identify the most effective properties of a general class of textures where the topology is comprised of a 2D lattice of scatterers; a particularly advantageous one is shown in Figure 1(a). This design is found to be effective in extracting light over a broad bandwidth and hence is potentially suitable for WOLEDs[17] used in solid-state lighting. Broad spectral out-coupling makes the design more challenging given that nanophotonic effects typically rely on coherent resonant phenomena that are restricted to narrow spectral bandwidths and preferred orientations.[18–20] Finally, we demonstrate that limited disorder in the array which is often encountered in fabrication can improve the out-coupling efficiency.

The optical properties of the WOLEDs were computed using full 3D electrodynamic simulations via MEEP—an open-source finite-difference time-domain (FDTD) software tool.[9] Using MEEP, we can compute the Poynting vector over a wide spectral bandwidth using a short temporal pulse, simulate a large supercell with its distributed-memory-parallelism and subpixel-smoothing features, and model the temporal dynamics of radiative exciton decay with nanometer-scale resolution using its customizable-source and pervasive-interpolation capabilities. We start with a planar, bottom-emitting WOLED comprised of four separate stacked layers: an Al cathode (thickness 100 nm), an organic film comprising hole-transporting (40 nm) and emissive (20 nm) and electron-transporting (40 nm) layers, an indium-tin oxide (ITO) transparent conductive film (100 nm), on top of a semi-infinite glass substrate with a square profile of length L, as shown in Figure 1(a). The refractive indices of the glass, organic, and ITO layers are $n_{glass} = 1.45$, $n_{ORG} = 1.8$, and $n_{ITO} = 1.8$, where losses in the ITO have been ignored since this layer is optically thin, and our primary focus is on plasmonic losses. The Al cathode is a lossy metal modeled using a Drude-Lorentzian fit that spans the WOLED emission spectrum.[21] We compute the wavelength-dependent total power emitted by ten different incoherent (i.e., random phase) electric point-dipole sources evenly distributed along a vertical line centered within the emissive layer (EML), in addition to the power in the glass, organic, and ITO layers (i.e., waveguide modes), the cathode/organic interface (i.e., surface-plasmon polaritons), and the absorption at the cathode. The ratio of the power in each of these components to the total

a)oskooi@umich.edu

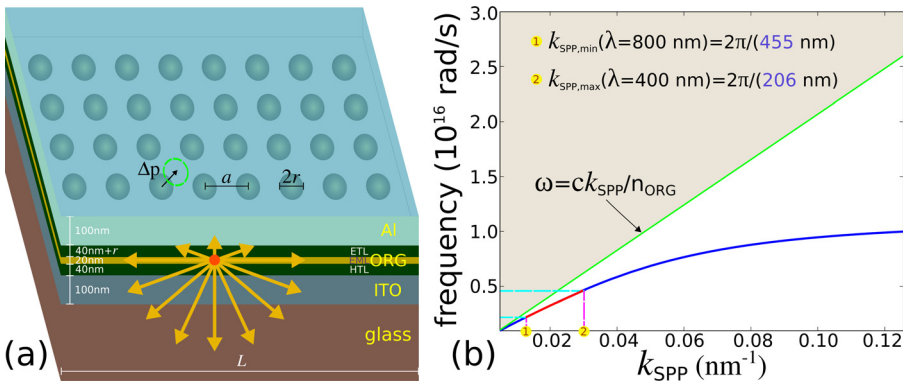

FIG. 1. (a) Schematic of a bottom-emitting OLED with a square profile of length L comprised of an aluminum (Al) cathode, electron-transporting (ETL) and emissive (EML) and hole-transporting (HTL) organic (ORG) layers, and indium-tin oxide (ITO) transparent anode, on top of a glass substrate. The thickness of each layer is marked. The surface of the ETL consists of a lattice with periodicity a of Al hemispheres with radius r protruding into the organic. Random disorder is introduced into the lattice by perturbing each hemisphere by an amount Δp whose values range between 0 and $\Delta\bar{p}$. Incoherent electric point-dipole sources are positioned within the EML to simulate the temporal dynamics of exciton recombination. (b) Dispersion relation of the SPP at the cathode/organic interface of the OLED. The red portion of the band corresponds to the operating range of white-emitting OLEDs: dashed lines extending from the frequency axis are modes with vacuum wavelengths of 400 nm to 800 nm with associated wavevectors ($2\pi/\lambda_p$, where λ_p is the wavelength of the plasma oscillation) noted on the horizontal axis. The shaded region is the light cone of the organic/ITO film.

dipole emission therefore gives the fraction of the total power that is distributed among the different device regions. Ten separate simulations are made, which provide sufficient convergence, for both planar and textured cathodes and the results averaged due to the random nature of the sources and in some cases the texture itself.

The total power emitted by a dipole source at a point in the EML is proportional to the local density of states (LDOS) at that point[22] which, in turn, is proportional to the rate of spontaneous emission obtained via Fermi's Golden Rule.[23–25] FDTD is used to compute the spontaneous-emission-rate enhancement factor defined as the ratio of the average power radiated per dipole in the nanostructured compared to the unpatterned device using identical coherent point sources in a single simulation. For calculations involving structures with textured surfaces, we use 16 000 electric-dipole emitters that are evenly distributed within a volume, centered within the EML, of rectangular cross-section of length a so as to sample the LDOS over the entire EML. In all cases, we use a resolution of 10 nm/pixel which, in combination with its subpixel-smoothing function, allows MEEP to model features whose scale is only a few nanometers.

Figures 2(a) and 2(b) show the simulated results for two orthogonal dipole orientations: parallel and perpendicular to the layers of an untextured WOLED with $L = 5\ \mu$m. Here, the total emitted power is separated into its components of glass, combined cathode/organic interface and organic/ITO waveguide (Al + ORG + ITO), and Al absorption. The average of

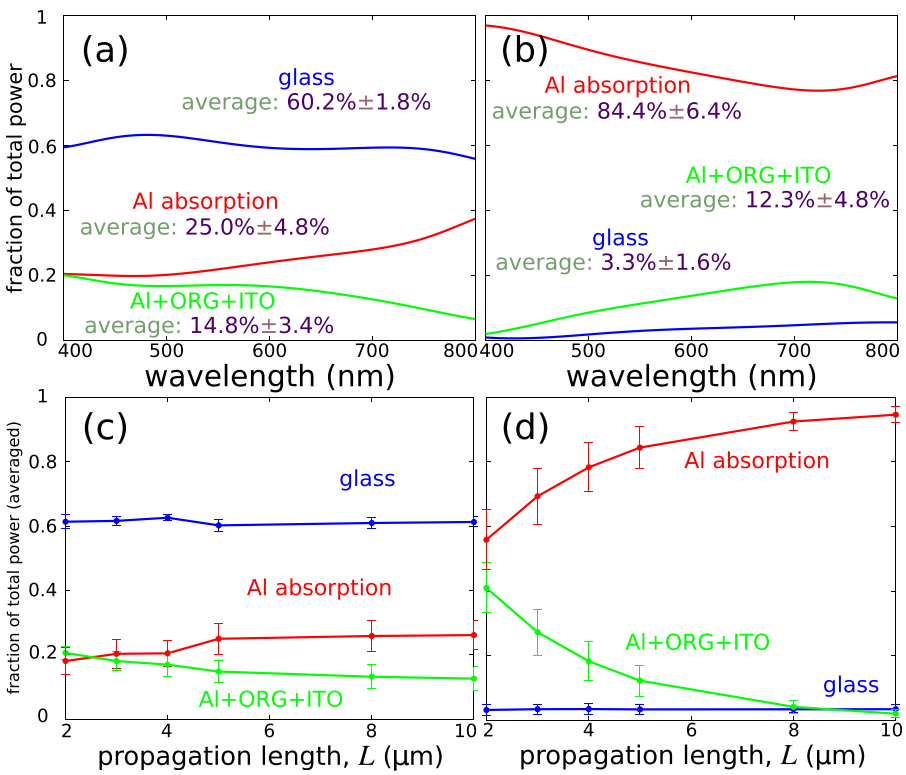

FIG. 2. Optical properties of a planar OLED. (a) and (b) Fraction of total dipole power in each of the three components of the OLED with $L = 5\ \mu$m: glass, combined cathode/organic interface and organic/ITO waveguide (Al + ORG + ITO), and Al absorption for (a) parallel and (b) perpendicular dipoles relative to the substrate plane. (c) and (d) Fraction of total dipole power, averaged over the wavelength spectrum, in the three device regions as functions of propagation length (L) under the cathode for dipoles with orientation (c) parallel and (d) perpendicular to the substrate plane. Losses in the metal due to the surface-plasmon polaritons are dominant.

each quantity over the entire wavelength interval is given, along with its standard deviation. We refer to the one pertaining to the glass as the light-extraction efficiency. As expected, the power reaching the glass is significantly less for perpendicular than for parallel dipoles (3% versus 60%), which is attributed to the large absorption losses of the Al cathode arising from SPPs[26] at the cathode/organic interface. Absorption losses from SPPs are still present for parallel dipoles but are much less significant (~25% of the total emission) than perpendicular ones (~84%). This is due to reduced coupling to SPPs as a result of mismatched electric-field boundary conditions for parallel dipoles, which suggests that large enhancements in the spontaneous-emission rate are possible for a non-planar, textured interface.[6,27,28]

The proportion of the total emission reaching the air assuming that the escaping light rays are isotropically incident on the planar glass-air interface is approximately $1/n_{glass}^2 \times \left(\frac{1}{3}P_\perp + \frac{2}{3}P_\parallel\right) \approx 20\%$, where $P_\perp$ and $P_\parallel$ are the emitted powers into the glass for perpendicular and parallel dipoles, respectively.[2,3] We plot the average power in each region as a function of propagation length under the cathode in Figures 2(c) and 2(d). The fraction of light absorbed by the Al cathode monotonically increases, whereas the waveguide component decreases with propagation length, indicating that most of the power outside the glass resides within the SPPs. For perpendicular dipoles, the Al absorption reaches approximately 95% of the total emission at $L = 10\,\mu$m, indicating that SPP losses are dominant for waveguide-mode propagation. Figures 2(c) and 2(d) also indicate that the SPP length is very short, and hence nanoscale texturing of the cathode surface can be effective in scattering the non-radiating SPPs.

An effective nanoscale texture should scatter all SPP modes into a direction *normal* to the interface while also increasing the spontaneous-emission rate. This requires that we identify such modes from their dispersion relation for the device and then determine the wavevector range across the emission spectrum of the WOLED. Some disorder may be necessary to ensure that the intrinsically narrowband resonant effects of ordered textures span the entire spectrum.[18–20,29] We can compute the dispersion relation for the WOLED configuration in Figure 1(a) by solving[30] $(\epsilon_1\epsilon_3 S_2^2 + \epsilon_2^2 S_1 S_3)\tanh(S_2 d) + \epsilon_2 S_2(\epsilon_3 S_1 + \epsilon_1 S_3) = 0$, where $S_i^2 = k_{SPP}^2 - \epsilon_i \omega^2/c^2$ and ϵ_i is the dielectric constant of the ith layer (i.e., $i=1$ is for the glass, $i=2$ is for the combined organic/ITO films, and $i=3$ is for the Al cathode), k_{SPP} is the wavevector of the SPP mode, ω is its angular frequency, c is the speed of light, and d is the thickness of the high-index organic/ITO layer (200 nm).

The SPP dispersion relation is shown in Figure 1(b). The light line of the organic/ITO film is also shown. The SPPs that lie below the line cannot couple to radiative modes within the light cone and thus are ultimately completely absorbed by the metal. The subset of modes within the WOLED are shown as the red portion of the blue-colored band where their corresponding group velocities, $\nabla_k \omega$, are relatively large compared to modes at larger wavevectors. This, in turn, results in a reduced DOS and hence a proportionately weaker effect on boosting the spontaneous-emission rate.[22] The dashed lines indicate modes with wavelengths of 400 nm and 800 nm that bound the usable emission spectrum of the WOLED. When these modes are expressed in terms of wavelengths of the plasma oscillation (λ_p), they are 206 nm and 455 nm, respectively. The SPP modes are therefore unaffected by intrinsic surface roughness having characteristic length scales of a few tens of nanometers,[31] which indicates that for effective scattering to occur, the surface must be carefully engineered. For the SPPs to scatter into radiation modes, momentum transfer is necessary via interaction with the cathode. If the in-plane wavevector component of the radiative mode (horizontal axis, Figure 1(b)) into which the SPP scatters is zero (i.e., $k_\parallel = k_{SPP} - k_{texture} = 0$), its out-of-plane wavevector component is then $k_\perp = \omega n_{ORG}/c$ and hence the mode scatters out normal to the layers. This suggests that to act as an effective grating out-coupler, the Fourier transform of the textured interface should span the full range of wavevectors for all SPPs in the plane.

This finding, therefore, provides a general criterion for texturing that can be met, for example, by a 2D square lattice of hemispherical scatterers protruding from the Al cathode into the ETL with periodicity a and radius r (see Figure 1(a)). Disorder is also controllably incorporated into the lattice via a perturbation Δp to each scattering site chosen randomly from a uniform distribution of values between 0 and $\overline{\Delta p}$ for both orthogonal in-plane directions. We also obtained similar results using cylindrical rods which suggest that the choice of scatterers can be potentially extended to other geometries including arbitrarily-shaped nanoparticles[28] or folds.[32] Such a general class of textures can be fabricated in vacuum-deposited organic films using, for example, embossing with either soft[33] or hard stamps,[34] as well as soft-contact removal approaches.[35] We have also investigated the case where dielectric scatterers protrude into the cathode and find that the out-coupling efficiency is significantly reduced in comparison, which is likely due to the smaller penetration of the SPP field into the metal than the dielectric.

Figure 3(a) shows results for perpendicularly-oriented dipoles for a WOLED with a surface texture array of total length $L = 10\,\mu$m with $a = 550$ nm, $r = 40$ nm, and $\overline{\Delta p} = 0$ (i.e., no disorder). To ensure consistency among designs with different textures, the distance between the EML and the patterned Al cathode is fixed at 40 nm independent of the hemisphere radius. In this case, the fraction of total emission reaching the glass is more than 15% (averaged over all wavelengths), which is nearly a factor of five greater than for the unpatterned case of Figure 2(b). Note, however, that there is a large variation of the extraction efficiency over the wavelength spectrum: small wavelengths have values above 30% while large wavelengths, where plasmon losses still dominate, have values less than 10%.

To understand why this hemispherical surface texture gives rise to an enhancement in the extraction efficiency, the Fourier transform of the height function, $|\tilde{h}(k_x, k_y)|$, is shown in Figure 3(c), where k_x and k_y are wavevectors. The spectral peaks of the array are evident, particularly in the region where the SPPs lie as denoted by the annular zone containing 20 peaks, 12 of which are distributed evenly in all radial directions *and* centered near the middle of the ring. This arrangement facilitates scattering of SPPs within a range of wavevectors of different magnitudes and directions into radiative states. This also explains why the extraction efficiency in Figure 3(a) is more pronounced at smaller than at larger

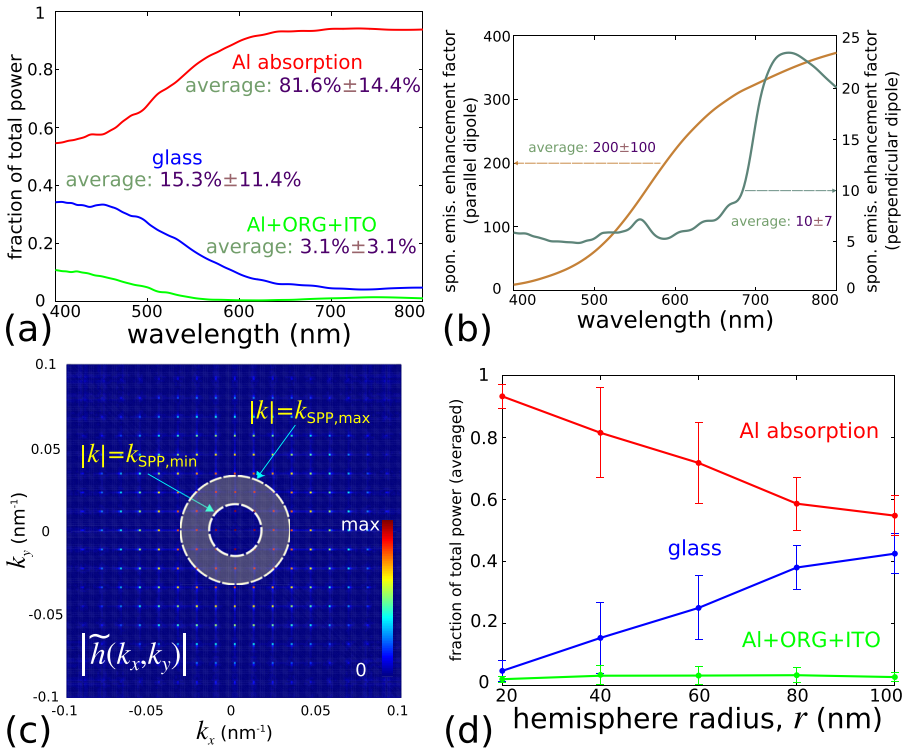

FIG. 3. (a) Fraction of total power of perpendicular dipoles in different device regions versus wavelength for a device with $L = 10\,\mu$m with an Al cathode consisting of a periodic lattice ($a = 550$ nm) of hemispheres ($r = 40$ nm) with no disorder. (b) Spontaneous-emission-enhancement factor of the nanostructured OLED relative to an unpatterned device versus wavelength for the two orthogonal dipole orientations: parallel (left vertical axis) and perpendicular (right). The average enhancement over the wavelength spectrum is shown. (c) Fourier transform of the height function of the surface texture, with the range of SPPs shown within the annular region. (d) Fraction of total power for perpendicular dipoles, averaged over the wavelength spectrum, in the three device regions as a function of hemisphere radius r with fixed $a = 550$ nm and no disorder. Results for parallel dipoles show a trend opposite to that of the Al absorption, increasing with r.

wavelengths, since the majority of the spectral peaks within the ring of Figure 3(c) lie closer to its outer boundary.

The effect of changing a, while keeping r and $\overline{\Delta p}$ fixed and thus shifting the *positions* of the peaks within the annular zone, has a significant effect on the scattering efficiency. When the spectral peaks are distributed either sparsely or unevenly within the annular zone, fewer SPPs are radiatively scattered leading to a reduction in the extraction efficiency. As an example, for $a = 150$ nm, 250 nm, 350 nm, 450 nm, and 650 nm, the efficiency enhancements are reduced in absolute terms by 4.4%, 4.0%, 6.1%, 6.6%, and 7.2%, respectively, relative to the optimal texture with $a = 550$ nm. The choice of a square lattice is arbitrary; any periodic arrangement of scatterers would have the same effect.

The spontaneous emission rate enhancement factor of both dipole orientations in Figure 3(b) shows noticeable gains. The enhancement is especially significant for parallel dipoles since the texture relaxes the electric-field boundary conditions that prevent coupling to the SPPs. This enhancement in spontaneous emission for parallel dipoles comes at the expense of a slightly reduced extraction efficiency (61.2% ± 1.6% for the unpatterned case versus 58.0% ± 8.2% for the lattice), which is more than offset by the gains for perpendicular dipoles (3.4% ± 1.4% versus 15.3% ± 11.4%). The presence of spectral features is evident for the perpendicular dipoles in Figure 3(b), particularly near 550 nm matching that of the lattice periodicity, which readily couple to SPP modes. The choice of a has a major impact on the spontaneous-emission rate for both dipole orientations as smaller lattice constants have larger enhancements than bigger ones due to an increased modulation of the surface.

Increasing the size of the scatterers and thus the amplitude of the spectral peaks also affects the light extraction efficiency, as shown in Figure 3(d). For $a = 550$ nm and no disorder, the extraction efficiency of perpendicular dipoles increases from 4.7% ± 3.5% to 42.5% ± 6.5% via a reduction in the Al absorption as the radius is increased from 20 nm to 100 nm or almost 13 times higher than for the unpatterned case. Even greater enhancements are possible using larger feature sizes. However, the plasmonic losses for parallel dipoles *increase* in the same interval (from 19.9% ± 2.7% to 35.0% ± 10.7%), indicating that there is an optimal value for r, of ~40 nm, which balances the gain for perpendicular with the loss for parallel dipoles. There is no such pronounced change in the spontaneous emission of perpendicular dipoles with increasing size of the hemispheres, although the parallel dipoles show a decrease, again indicating that smaller scatterers are preferable.

Figure 4 shows $h(x, y)$ of the Al cathode and a 1D cross-section of its Fourier transform, $|\tilde{h}(0, k_y)|$, for $a = 550$ nm and $r = 40$ nm having three different disorder parameters $\overline{\Delta p}$. For a lattice with a limited disorder of $\overline{\Delta p} = 0.05a$, the average extraction efficiency of perpendicular dipoles is increased by 1.3% absolute and 8.5% relative beyond that of the unperturbed lattice due to the slight *broadening* of the spectral peaks which increases the number of scattered SPPs. However, for $\overline{\Delta p} > 0.05a$, the effect of the broadening is outweighed by the reduction in peak amplitude which results in a decrease of the extraction efficiency. A highly disordered lattice texture lacking spectral features still outperforms a smooth interface given that some degree of scattering remains. Similar results were found for parallel dipoles. The enhancements beyond the unperturbed lattice obtained with limited disorder are even greater with larger scatterers. The tradeoff in the peak amplitude vs. width via partial disorder can therefore be used to increase the light-extraction efficiency beyond that of any perfectly periodic surface texture. Partial disorder, however, has little effect on the spontaneous-emission rate, since the DOS is unaffected. Disorder also, as expected, reduces the variation in the

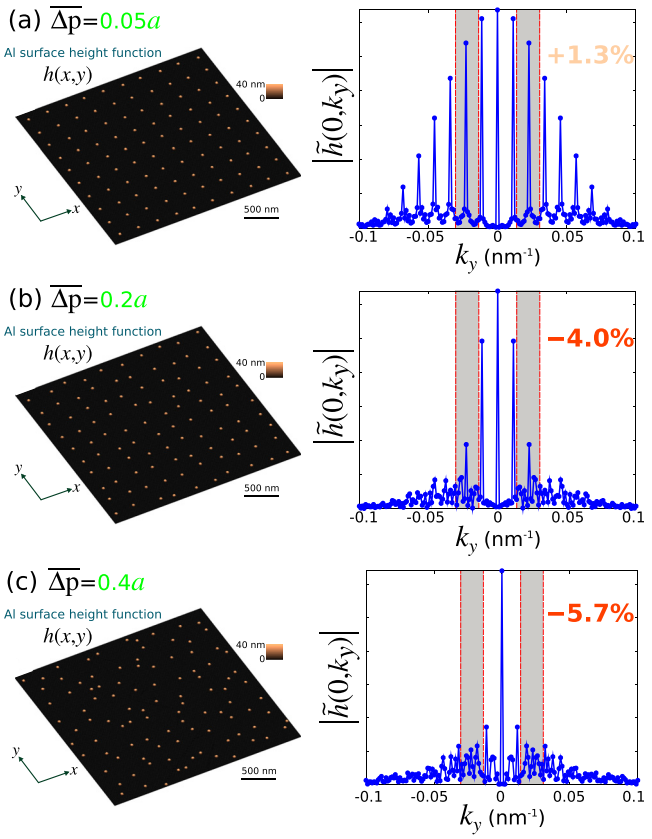

FIG. 4. Schematic of the surface height function of the cathode and a 1D cross section of its corresponding Fourier transform (with the wavevectors of the SPP modes shown in the gray region) for three different cathode lattice arrays with $a = 550$ nm and $r = 40$ nm, where the disorder $\bar{\Delta p}$ is: (a) 0.05a, (b) 0.2a, and (c) 0.4a. For $\bar{\Delta p} = 0.05a$, the average extraction efficiency for perpendicular dipoles is increased by 1.3% absolute and 8.5% relative beyond the unperturbed lattice due to the slight broadening of the peaks. Further increases in the disorder result in the elimination of the peaks and hence a reduction in the extraction efficiency. In the limit of large disorder where no traces of the peaks remain, the extraction efficiency is still enhanced beyond that of an unpatterned interface. Results for parallel dipoles show similar trends.

extraction efficiency over the wideband spectrum: for perpendicular dipoles, the standard deviation of the averaged extraction efficiency is reduced monotonically by 5.2% absolute for $\overline{\Delta p} = 0.4a$ compared to the unperturbed case. Peak broadening arising from lattice disorder can also be realized by introducing small non-uniformities into the size and morphology of the scatterers, which again can be used to extend the range of applicable textures.

In summary, we have shown how texturing of the metal-cathode surface using a topology based on a 2D lattice of scatterers can be used to reduce losses from SPPs and enhance both the light-extraction efficiency and the spontaneous-emission rate of excitons in WOLEDs compared with an unpatterned device. The choice of the morphology of the scatterers and the topology of the lattice has some degree of flexibility although their exact dimensions must be carefully tuned to optimize device performance. Our design does not require any additional materials and hence can be used to explore optimal designs for different OLED layering schemes and emission spectra. Texturing of the cathode surface based on the designs presented in this work may potentially lead to marked improvements in the overall efficiency of OLEDs.

We thank Professor Stephen R. Forrest at the University of Michigan for numerous helpful comments and suggestions. We are also grateful to Brock Palen of the Center for Advanced Computing for technical assistance with running MEEP on the Flux high-performance cluster and to Behrouz Shiari for access to the NNIN/C computing resources at the UofM. This work also made use of the Extreme Science and Engineering Discovery Environment (XSEDE) at the Texas Advanced Computing Center, which was supported by National Science Foundation (Grant No. ACI-1053575). This work was partially supported by Universal Display Corp.

[1]M. A. Baldo, D. F. O'Brien, Y. You, A. Shoustikov, S. Sibley, M. E. Thompson, and S. R. Forrest, Nature **395**, 151 (1998).
[2]K. Saxena, V. K. Jain, and D. S. Mehta, Opt. Mater. **32**, 221 (2009).
[3]W. Brutting, J. Frischeisen, T. D. Schmidt, B. J. Scholz, and C. Mayr, Phys. Status Solidi A **210**, 44 (2013).
[4]V. Bulovic, V. B. Khalfin, G. Gu, P. E. Burrows, D. Z. Garbuzov, and S. R. Forrest, Phys. Rev. B **58**, 3730 (1998).
[5]S. Nowy, B. C. Krummacher, J. Frischeisen, N. A. Reinke, and W. Brutting, J. Appl. Phys. **104**, 123109 (2008).
[6]G. Sun, J. B. Khurgin, and R. A. Soref, Appl. Phys. Lett. **90**, 111107 (2007).
[7]K. Y. Yang, K. C. Choi, and C. W. Ahn, Appl. Phys. Lett. **94**, 173301 (2009).
[8]M. Furno, R. Meerheim, S. Hofmann, B. Lussem, and K. Leo, Phys. Rev. B **85**, 115205 (2012).
[9]A. F. Oskooi, D. Roundy, M. Ibanescu, P. Bermel, J. D. Joannopoulos, and S. G. Johnson, Comput. Phys. Commun. **181**, 687 (2010).
[10]*Advances in FDTD Computational Electrodynamics: Photonics and Nanotechnology*, edited by A. Taflove, A. Oskooi, and S. G. Johnson (Artech House, Boston, 2013).
[11]W. L. Barnes, J. Mod. Opt. **45**, 661 (1998).
[12]J. M. Lupton, B. J. Matterson, I. D. W. Samuel, M. J. Jory, and W. L. Barnes, Appl. Phys. Lett. **77**, 3340 (2000).
[13]P. A. Hobson, S. Wedge, J. A. E. Wasey, I. Sage, and W. L. Barnes, Adv. Mater. **14**, 1393 (2002).
[14]U. Geyer, J. Hauss, B. Riedel, S. Gleiss, U. Lemmer, and M. Gerken, J. Appl. Phys. **104**, 093111 (1998).
[15]J. Frischeisen, Q. Niu, A. Abdellah, J. B. Kinzel, R. Gehlhaar, G. Scarpa, C. Adachi, P. Lugli, and W. Brutting, Opt. Express **19**, A7 (2010).
[16]C. S. Choi, D.-Y. Kim, S.-M. Lee, M. S. Lim, K. C. Choi, H. Cho, T.-W. Koh, and S. Yoo, Adv. Opt. Mater. **1**, 687 (2013).
[17]Y. Sun, N. C. Giebink, H. Kanno, B. Ma, M. E. Thompson, and S. R. Forrest, Nature **440**, 908 (2006).
[18]A. Oskooi, P. Favuzzi, Y. Tanaka, H. Shigeta, Y. Kawakami, and S. Noda, Appl. Phys. Lett. **100**, 181110 (2012).
[19]A. Oskooi, Y. Tanaka, and S. Noda, Appl. Phys. Lett. **104**, 010121 (2014).
[20]A. Oskooi, M. De Zoysa, K. Ishizaki, and S. Noda, ACS Photonics **1**, 304 (2014).
[21]A. D. Rakic, A. B. Djurisic, J. M. Elazar, and M. L. Majewski, Appl. Opt. **37**, 5271 (1998).
[22]A. Oskooi and S. G. Johnson, "Electromagnetic wave source conditions," in *Advances in Computational Electrodynamics: Photonics and Nanotechnology* (Artech, Boston, 2013), Chap. 4.
[23]P. W. Milonni, Phys. Rep. **25**, 1 (1976).
[24]F. Wijnands, J. B. Pendry, F. J. Garcia-Vidal, P. M. Bell, P. J. Roberts, and L. M. Moreno, Opt. Quantum Electron. **29**, 199 (1997).
[25]Y. Xu, R. K. Lee, and A. Yariv, Phys. Rev. A **61**, 033807 (2000).
[26]H. Raether, *Surface Plasmons on Smooth and Rough Surfaces and on Gratings* (Springer-Verlag, New York, 1988).
[27]R. M. Amos and W. L. Barnes, Phys. Rev. B **59**, 7708 (1999).
[28]E. Fort and S. Gressilon, J. Phys. D: Appl. Phys. **41**, 013001 (2008).
[29]J. B. Khurgin and G. Sun, Appl. Phys. Lett. **94**, 221111 (2009).
[30]J. Burke, G. Stegeman, and T. Tamir, Phys. Rev. B **33**, 5186 (1986).
[31]K. Okamoto, I. Niki, A. Shvartser, Y. Narukawa, T. Mukai, and A. Scherer, Nat. Mater. **3**, 601 (2005).
[32]W. H. Koo, S. M. Jeong, F. Araoka, K. Ishikawa, S. Nishimura, T. Toyooka, and H. Takezoe, Nat. Photonics **4**, 222 (2010).
[33]D. Qin, Y. Xia, and G. M. Whitesides, Nat. Protocols **5**, 491 (2010).
[34]L. J. Guo, Adv. Mater. **19**, 495 (2007).
[35]C. E. Packard, K. E. Aidala, S. Ramanan, and V. Bulovic, Langmuir **27**, 9073 (2011).